Sensors & Diagnostics

PAPER

View Article Online
View Journal | View Issue

Cite this: *Sens. Diagn.*, 2025, **4**, 247

A new perspective on the AIE and ACQ of phosphinine-anchored luminescent materials as visual and ratiometric sensors for Ag^+ and Hg^{2+} ion detection in live cells†

Saravanan Enbanathan, [a] Umamahesh Balijapalli, [b] Manojkumar Dhanthala Thiyagarajan, [b] Selin Manojkumar, [a] Saravanakumar Manickam [c] and Sathiyanarayanan Kulathu Iyer *[a]

The effective synthesis of phosphinine-based (*E*)-2-((2,6-dicyano-1,1-diphenyl-λ^5-phosphinin-4-yl) methylene) hydrazine-1-carbothioamide (**MHC**) and (*E*)-4-((2-(benzo[*d*]thiazol-2-yl)hydrazineylidene) methyl)-1,1-diphenyl-λ^5-phosphinine-2,6-dicarbonitrile (**BHP**) sensor materials resulted in the characterization of their notable photophysical characteristics, including aggregation, solvatochromism, and sensing ability. Upon application, the ratiometric emission properties of the **MHC** and **BHP** probes were evaluated, and they exhibited noteworthy selectivity and sensitivity for silver (Ag^+) and mercury (Hg^{2+}) ions over other metal ions. After conducting a thorough photophysical investigation, the detection limits (LODs) for Ag^+ and Hg^{2+} were determined to be as low as 8.7 and 8.6 nM for **MHC** and 280 and 340 pM for **BHP**, respectively. In addition, **MHC** and **BHP** were examined as capable sensing materials for Ag^+ and Hg^{2+} ions on paper strip-based sensors and bio-images. ^{1}H NMR titration, HRMS analysis and DFT studies validated the binding processes of **MHC** and **BHP** with Ag^+ and Hg^{2+} ions. These findings contribute to the future development of practical onsite detection of Ag^+ and Hg^{2+} ions in ecological systems.

Received 8th November 2024,
Accepted 11th January 2025

DOI: 10.1039/d4sd00345d

rsc.li/sensors

1. Introduction

There is an increasing demand for the development of optically active molecules that can specifically detect several small molecules, neutral molecules, cations and anions that are important in biological, environmental, and industrial processes.[1–5] These tools could solve several forensic, toxic, and ecological remediation problems at a reasonable cost. Owing to their ease of use, affordability, selectivity, and sensitivity detection up to the ppm/ppb level, detection methods based on fluorescent and optical technologies have been extensively investigated in this respect.[6–8] Silver (Ag^+) and mercury (Hg^{2+}) ions are two transition metal ions that have gained significant interest. The effectiveness of Ag^+ ion sensors, despite the efforts of several researchers, is lower than that of sensors for other metal ions. Due to the widespread use of Ag^+ ions in photography, electronics, cosmetics, antibacterial agents and pharmaceutical applications, millions of tonnes of trash containing Ag^+ ions are released into the environment each year, contaminating water supplies.[9,10] The Secondary Potable Water Standards of the Environmental Protection Agency (EPA) set 0.1 μg mL^{-1} as the maximum allowable concentration of Ag^+ ions in potable water systems. Overconsumption and prolonged build-up of Ag^+ ions can result in the formation of insoluble precipitates in the skin and eyes. Regular exposure to Ag^+ ions in animals can lead to anaemia, growth retardation, heart hypertrophy, and degenerative alterations, which have adverse impacts on humans.[11,12] Ag^+ ions can inactivate enzymes and significantly disrupt biological systems by binding to thiol, amino, and carboxyl groups in enzymatic processes and/or displacing other essential metallic ions. In addition, exposure to Ag^+ ions leads to bioaccumulation, which has undesirable impacts on living beings.

Hg^{2+} ions are one of the crucial heavy metals found in soil, water, and the surrounding environment due to industrialization, thermal power plants, the burning of fossil fuels, laboratory activities, and other sources.[13–15] It is considered the most hazardous metal ion to humans among

[a] *Department of Chemistry, School of Advanced Sciences and Vellore Institute of Technology, Vellore-632 014, India. E-mail: sathiya_kuna@hotmail.com*
[b] *Centre for Organic Photonics and Electronics Research (OPERA) and Department of Applied Chemistry, Kyushu University, 744 Motooka, Nishi, Fukuoka, 819-0395 Japan. E-mail: umahesh083@gmail.com*
[c] *Department of Materials Science and Engineering, University of Utah, Salt Lake City, 84112, UT, USA*

† Electronic supplementary information (ESI) available. See DOI: https://doi.org/10.1039/d4sd00345d

the heavy transition metal ions. The World Health Organisation (WHO) and the United States Environmental Protection Agency (U.S. EPA) suggest a limit of 2 parts per billion (ppb) or 0.002 μg mL^{-1} of Hg^{2+} ions in drinking water.[16] Hg^{2+} ions and pollutants may readily penetrate the tissues, cell membrane, and respiratory system due to their extremely reactive nature and liposolubility. Hg^{2+} ions can accumulate in human tissues through the food chain. Even at extremely low concentrations, it may gather in the human body and cause significant, long-lasting harm to the kidneys, brain, central nervous system, and immune system.[17–20] Therefore, a sensitive, quick, and accurate analytical method is much needed to determine Hg^{2+} ions in environmental, nutritional, and biological resources.

Consequently, the development of sensitive and selective techniques for the detection of Ag^{+} and Hg^{2+} ions in semi aqueous solutions is crucial. Several research groups have attempted to create fluorescence sensors for the identification of Ag^{+} and Hg^{2+} ions using tetraphenylethene,[21] thiourea,[22] 4-hydroxybenzaldehyde[23] and triarylamine rhodanine.[24] Ag^{+} and Hg^{2+} ions have recently been detected using inductively coupled plasma mass spectrometry, gas chromatography, atomic absorption spectrometry, and high-performance liquid chromatography.[25–27] Unfortunately, there has not been widespread use of the traditional approaches indicated above owing to rising equipment charges and complicated operational processes. In addition to superior sensitivity, excellent selectivity, cheap cost, real-time sensing, and ease of employing them, colorimetric and fluorescence techniques are gaining popularity as tools for identifying and analysing small quantities of analytes. Several fluorescent probes have been utilised in recent literature to detect Ag^{+} and Hg^{2+} ions in environmental and biological materials. Regrettably, the limited sensitivity and high limit of detection (LOD) of these light probes restrict their practical use. The aforementioned obstacles and the potential uses of luminous chromophores make it possible to construct cutting-edge and unique luminous probes with numerous additional benefits for use in biological, environmental, and pharmaceutical research. Additionally, there are no studies on the use of a single fluorescence probe to detect both the metal ions in a ratio metric detection approach.

Diphenyl-λ^5-phosphinine (PDC) and its derivatives are a family of highly fluorescent dyes with remarkable optical, environmental, and thermal stability. Recently, interest in using these dyes in organic lasers[28] and OLEDs[29] has grown enormously. Researchers have an inclination towards thioureas and benzothiazole derivatives because of their wide range of applications in various fascinating fields.[22,30–34] The existence of nitrogen and sulphur donor atoms in the thiourea and benzothiazole backbones affects a wide range of binding options. To create stable complexes, they should subsequently coordinate with metal centres. We develop aggregation-based optical chemosensors containing phosphinine moiety with the conjugation of thiosemicarbazide and benzothiazole units. The photophysical and solvatochromism features of **MHC** and **BHP** are analysed. The noteworthy features of both **MHC** and **BHP** sensors are their distinct fluorescent characteristics, which are attributed to their comparable binding nature to attract Ag^{+} and Hg^{2+} ions with distinct spectrum features. **MHC** exhibits a blue shift using the chelation enhancement fluorescence effect (CHEF) mechanism. In contrast, the chelation enhancement quenching effect (CHEQ) causes a red shift in **BHP**. Using Whatman filter paper, we created a probe, **MHC** and **BHP** strip to successfully detect Ag^{+} and Hg^{2+} ions on-site. These sensors are used for environmental analysis and bio-imaging in living HeLa cells.

2. Results and discussion

The synthesis of **MHC** and **BHP** involves relatively a few different synthetic steps, which are summarised in Scheme 1. Bis(cyanomethyl)diphenyl phosphonium chloride (**step-1**) and *N*,*N*′-diphenyl-1,3-diiminopropane (**step-2**) were used as the starting materials. Through a series of processes, the intermediate 1,1-diphenyl-1-λ^5-phosphinine-2,6-dicarbonitrile (**PD**) was produced (**step-3**). Under Vilsmeier–Haack conditions (**step-4**), **PD** was formylated with $POCl_3$ and DMF, which led to good quantities of a 4-formyl **PD** product (**PDC**). Using thiosemicarbazide (**step-5**) and 2-hydrazinobenzothiazole (**step-6**), a C═N isomerization product was formed, and the formyl group was converted into an imine group, which was then used to produce the target sensors **MHC** and **BHP**. The recrystallization technique and column chromatography were used to purify all the active components. This is because both target compounds dissolve readily in common organic solvents, such as dimethyl sulfoxide, toluene, dichloromethane, acetone, and acetonitrile, making it simpler to test their ability to detect them. Through ^{1}H NMR, ^{13}C NMR, ^{31}P NMR, and HRMS analysis, the chemical structures of the products, **PD**, **PDC**, **MHC**, and **BHP**, were thoroughly identified (ESI† Fig. S1–S14).

2.1. Solvatochromism

As shown in Fig. 1, we examined the solvatochromism of the compounds **MHC** and **BHP** in non-polar to polar solvents at a concentration of 2×10^{-5} M. As shown in ESI† Fig. S15a (**MHC**) and S15b (**BHP**), and Table S1, minor and maxima absorption

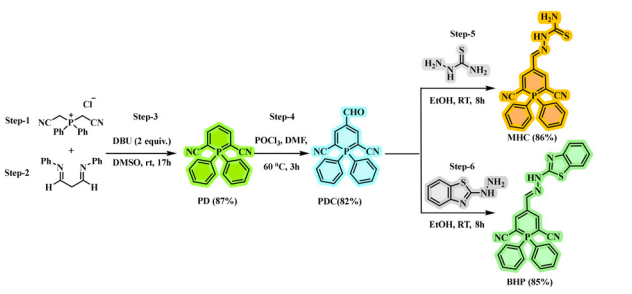

Scheme 1 Synthetic method for producing the target sensors **MHC** and **BHP**.

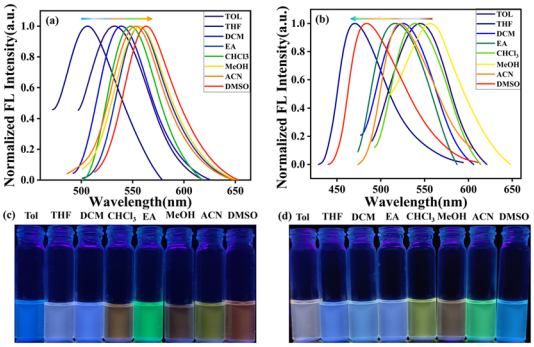

Fig. 1 (a and b) Normalized fluorescence spectra of the solutions of **MHC** and **BHP** in different solvents (non-polar to polar). (c and d) Fluorescence bottle images of **MHC** and **BHP** under portable UV light radiation (365 nm) in various solvents, such as Tol – toluene; THF – tetrahydrofuran; DCM – dichloromethane; EA – ethyl acetate; $CHCl_3$ – chloroform; MeOH – methanol; ACN – acetonitrile; DMSO – dimethyl sulfoxide.

changes imply a stable ground state when solvent polarity increases from Tol to DMSO. However, the fluorescence emission response of **MHC** was sensitive to the polarity of the solvent. When the polarity of the solvent changed from non-polar to vastly polar DMSO (Fig. 1a), **MHC** showed a large solvatochromic effect with a large bathochromic change in its emission, which formed a positive solvatochromism. As the polarity of the solvent increased, the fluorescence colour of the **MHC** solution under UV illumination changed from blue to orange in various solvents. Fig. 1c depicts the observed colour shifts in emission in different solvents. In contrast, **BHP** exhibited negative solvatochromism, with its absorbance shifting from longer (338 nm) to shorter (346 nm) wavelengths when the polarity of the solvent changed from non-polar to polar. The longest emission wavelength was shown by a nonpolar solvent, such as toluene at 547 nm, while the shortest wavelength was displayed by a polar solvent, such as DMSO, at 485 nm. It arose from solute–solvent interactions inside the molecule at a highly dipolar ground state. Additionally, this seems to be connected to the charge-transfer event that occurs between the phosphinine unit and the benzothiazole substituents and whether it is radiative *vs.* non-radiative. As the polarity of the solvent increases, **BHP** undergoes a significant blue shift in accordance with negative solvatochromism. Even though DMSO has a much higher refractive index than the less polar toluene, a hypsochromic effect was observed when the solution was changed from toluene to DMSO. A bottle picture of **BHP** in various solvents is shown in Fig. 1d. The Lippert–Mataga plot is illustrated in ESI† Fig. S16 shows a linear association between Stokes shifts and orientation polarizability. It was, therefore, possible to understand the solvatochromic properties of **MHC** and **BHP** using the Lippert–Mataga mode. The findings demonstrated the feasibility of using **MHC** and **BHP** to differentiate between organic solvents. All these tests demonstrated that ICT occurred inside the **MHC** molecule as a result of photoexcitation.

2.2. Aggregation studies

The possibility of the **MHC** and **BHP** molecules coming together to form aggregates was also studied by utilising solvent mixtures consisting of varying amounts of tetrahydrofuran and water. As the ratio of THF to water in the solution changed, the fluorescence maxima migrated progressively to the redshift by 5 nm (Fig. 2a). Meanwhile, there were many strong fluorescent coarse precipitate forms in the mixture, and the fluorescent colours changed from light yellow to orange. All the mixtures became homogeneous suspensions without any precipitate or suspension forming when water was added to THF; a characteristic feature frequently observed for AIEgens, and the fluorescent colours ultimately changed to orange with a water fraction of 90 volume%. However, the intensity of the fluorescence increased when the water fraction was increased to 90%. In comparison (Fig. 2b), **BHP** shows that when the water content rose from 0 to 100%, the strength of the emissions decreased. However, the majority of the typical organic fluorescent probes used in these studies self-quenched when exposed to increasing concentrations, resulting in a decrease in fluorescence intensity. This is called the "ACQ effect". To represent the degree of aggregation, a rational plot illustrating the fluorescence intensity ratio (I_{509} and I_{469}) *versus* water fractions (0–100%) is presented (Fig. 2c and d). Fig. 2c shows a 2.6-fold increase in fluorescence intensity as the water fraction increases from 0 to 90%. Conversely, Fig. 2d depicts a 3.5-fold decrease in intensity when the water fraction increases from 0 to 100%.

2.3. UV-visible absorption and emission study of MHC and BHP

The mechanistic aspects of the metal ion-probe interaction were investigated through UV-visible absorption and fluorescence studies. The detecting capacity of the **MHC** and **BHP** receptors was studied by adding 1×10^{-3} M (10 equivalents) of different metal ions, such as Ba^{2+}, Ca^{2+}, Cu^{2+}, Cd^{2+}, Li^{+}, Fe^{2+}, Fe^{3+}, Na^{+}, K^{+}, Mg^{2+}, Ni^{2+}, Cr^{3+}, Ag^{+} and Hg^{2+}, in aqueous solution. Fig. 3a and b show the UV-visible

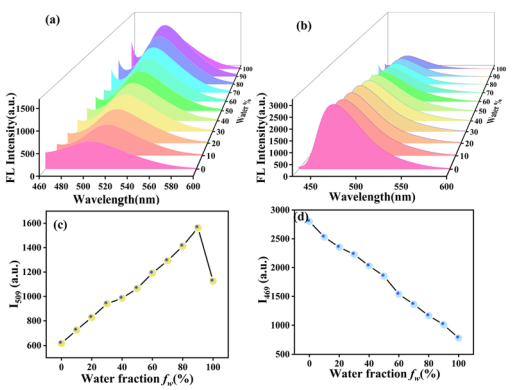

Fig. 2 (a and b) 3D fluorescence emission spectra of **MHC** and **BHP** (2×10^{-5} M) in THF/H_2O (0–100%). (c and d) Plots of I_{509} nm and I_{469} values *versus* water fraction% of the solvent system in **MHC** and **BHP**.

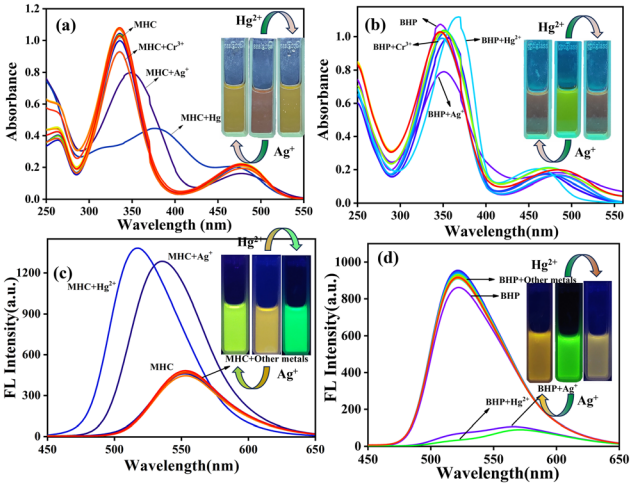

Fig. 3 UV-visible absorbance selectivity spectra of the sensors (a) **MHC**, (b) **BHP** and fluorescence emission selectivity spectra of (c) **MHC** and (d) **BHP** in the presence of various metal ions (1×10^{-3} M, 10 equivalents) in ACN : H_2O (8 : 2) solutions. The addition of Ag^+ and Hg^{2+} ions caused noticeable naked-eye color changes in **MHC** and **BHP**, as shown in (a) and (b), along with fluorescence color changes depicted in (c) and (d).

absorption and fluorescence spectra, which depict that Ag^+ and Hg^{2+} ions in ACN : H_2O (8 : 2) solutions can be detected more easily and selectively than other cations. When Ag^+ ions are present, the π–π* absorption peak of **MHC** shifts slightly to the red, moving from 340 to 350 nm. However, when Hg^{2+} ions are present, the peak moves from 340 to 390 nm. When compared to Ag^+ and Hg^{2+} ions, the spectral alterations caused by Cr^{3+} ions are less dramatic, even though they result in a notable drop in the strength of the peak at 340 nm and a wider absorption spectrum. Fig. 3a shows that when Ag^+ and Hg^{2+} are added to the light red **MHC** solution, the solution changes to a yellowish colour, which can be observed with the naked eye. Under the 365 nm UV lamp, the solution's vivid orange fluorescence of **MHC** changed to a strong yellowish-green fluorescence when the Ag^+ ion was present; similarly, Hg^{2+} altered colour from yellowish orange to green. The fluorescence of **MHC** shifted 17 nm to the blue side by exposure to Ag^+ ions, which resulted in an increase in **MHC** fluorescence. However, Hg^{2+} also enhanced the fluorescence of the receptor, with only slight blue shifts of 36 nm in **MHC** to attain maximum fluorescence intensity. Therefore, it follows that the receptor **MHC** preferentially recognises both Ag^+ and Hg^{2+} ions, although with separate signals for each species, as shown above. Interestingly, we observed the dramatic fluorescence transitions from yellowish orange to yellowish green (Ag^+) and green (Hg^{2+}). Metal ion binding to S and N atoms in thiosemicarbazide (TSC) is the source of the spectrum shifts. We made another sensor, **BHP**, which had a benzothiazole molecule and acted as an acceptor. This was done to learn more about how binding works and to see if there was any coordination in binding. Understanding the binding of metal ions to molecules replaced with numerous receptors combined with a single signalling unit is easier by molecular design. In the presence of Ag^+ and Hg^{2+} ions, the bright green ACN : H_2O (8 : 2) solution of **BHP** became deep orange, which is visible to the naked eye (Fig. 3c). The presence of Ag^+ ions reduces the intensity of the greatest energy absorption, and the fluorescence emission band exhibits a wavelength at 350 nm. In the presence of Hg^{2+} ions, **BHP** showed a slight red shift in its absorption by 22 nm, but its fluorescence was dramatically red-shifted with decreasing intensity, exhibiting a shift of 51 nm and a new peak at 573 nm. All the sensors were able to distinguish between Ag^+ and Hg^{2+} ions. However, the amount of colour and spectral change depended on the number of acceptor moieties. This was done by measuring the fluorescence spectra of sensor-Ag^+ and Hg^{2+} ions in the presence of other metal ions in an ACN : H_2O (8 : 2) solution.

Because the binding was evaluated by changes in their electronic characteristics, it is crucial to comprehend the UV-visible absorption and fluorescence spectra of the receptors in ACN : H_2O (8 : 2) solution shown in ESI† Fig. S17. Both the **MHC** and **BHP** sensors showed strong absorption across a wide wavelength range, from the ultraviolet to the middle of the visible spectrum, with the highest energy maxima occurring at 480 and 468 nm. The phosphinine groups linked with the TSC core through prolonged conjugation considerably affected the transition from the lowest-energy singlet state (S_0) to the first excited singlet state (S_1), which was responsible for the lowest energy absorption. Evidence of the participation of intramolecular charge transfer in **MHC**, from the donor TSC to the acceptor phosphinine moiety was observed in the substantially greater Stokes shift value of 11 502 cm^{-1}. Therefore, the preferential signalling route towards Ag^+ and Hg^{2+} ions was disrupted as a consequence of the metal ion binding.

2.4. FL titration spectroscopy

The fluorescence titration spectra depicted in Fig. 4 demonstrate the ratio-metric discrimination of **MHC** and **BHP** over Ag^+ and Hg^{2+} ions. The samples were excited at the corresponding isosbestic point shown in the UV-visible absorption titration spectra to analyse the spectra. In Fig. 4a and b, **MHC** emission titration shows a blue shift from 553 nm to 536 nm for Ag^+ ion and 553 nm to 517 nm for Hg^{2+} with increasing emission intensity. In addition, a red shift from 522 nm to 570 nm and 573 nm for Ag^+ and Hg^{2+} ions with decreasing emission spectra in **BHP** (Fig. 4e and f) was observed with increased concentrations of Ag^+ and Hg^{2+} ions (0–2 equivalents) in ACN : H_2O (8 : 2) solution system. This linear calibration plot was created using data from an analysis of FL emission titration. The limit of detection (LOD) using the fluorescence intensities of the **MHC** and **BHP** receptors was found using the calibration curve formula LOD = $(3 \times \sigma)$/slope. We found a remarkable linear connection between the relative fluorescence intensities and analyte concentrations using the calibration curve. Using the emission measurements of 10 blank samples to determine the relative

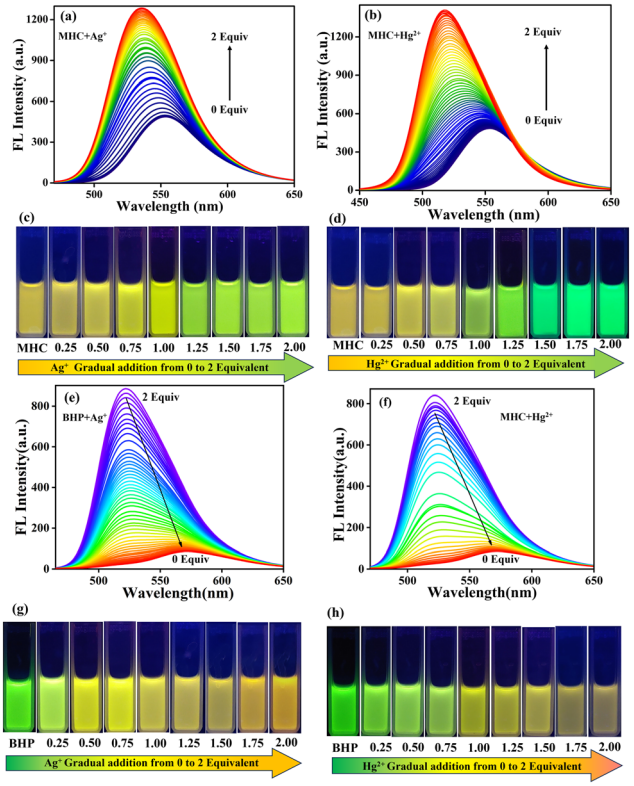

Fig. 4 Fluorescence emission titration spectra of **MHC** (a and b) and **BHP** (e and f) (2×10^{-5} M) with the gradual addition of Ag^+ and Hg^{2+} ions in ACN : H_2O (8 : 2) solution (0–2 equivalents). The gradual addition of Ag^+ ions (0–2 equivalents) (c and g) and Hg^{2+} ions (0–2 equivalents) (d and h) was performed under a UV lamp emitting at 365 nm.

standard deviation (σ), the LOD was found to be 8.7 nM and 280 pM for Ag^+ ions in **MHC** and **BHP**, respectively (ESI† Fig. S18). However, the limit of detection (LOD) for Hg^{2+} ions in **MHC** and **BHP** was limited to 8.6 nM and 340 pM, respectively (ESI† Fig. S19). This was much lower than what had been reported in previous investigations (ESI† Table S2). The sensor's detection limit is sufficient to identify the presence of Ag^+ and Hg^{2+} ions in water that exceeded the permitted limits. Fig. 4c and d illustrate the progressive addition of Ag^+ and Hg^{2+} ions in the solution state from 0 to 2 equivalents. While increasing the amount of Ag^+ in **MHC**, the emission colour changed from yellowish-orange to yellow-green. In the same way, Hg^{2+} changed from yellowish orange to green. Additionally, in (Fig. 4g and h), to **BHP**'s progressive addition of Ag^+ and Hg^{2+} from 0 to 2 equivalents, the observed colour changed from bright green to orange in Ag^+ and bright green to reddish-orange in Hg^{2+} ions.

2.5. Interference and time-dependent studies

To evaluate the selectivity of the sensors in sensing Ag^+ and Hg^{2+} ions, the fluorescence spectra of sensors **MHC**/**BHP**-Ag^+/Hg^{2+} complexes in ACN : H_2O (8 : 2) solution were measured in the presence of various metal ions, and the results are shown as a bar chart, as shown in (ESI† Fig. S20). Interestingly, the presence of other metal ions, such as Ba^{2+}, Ca^{2+}, Cu^{2+}, Cd^{2+}, Li^+, Fe^{2+}, Fe^{3+}, Na^+, K^+, Mg^{2+}, Ni^{2+}, and Cr^{3+} had no effect, indicating that all the compounds disclosed here specifically did not affect the detection of the Ag^+ and Hg^{2+} ions in ACN : H_2O (8 : 2) solutions. Moreover, when both Ag^+ and Hg^{2+} ions were added simultaneously, the fluorescence spectrum (ESI† Fig. S21) resembled that of Hg^{2+} alone, suggesting that Hg^{2+} has a higher binding affinity with the sensor than Ag^+. The binding constants (K_a) of the sensor-Ag^+/Hg^{2+} complexes were calculated using the Benesi–Hildebrand (B–H) equation: K_a = intercept/slope, which were found to be 2.28×10^8 M^{-1} and 1.77×10^8 M^{-1} for Ag^+ and Hg^{2+} ions in **MHC** (ESI† Fig. S22) and 1.27×10^8 M^{-1} and 2.24×10^8 M^{-1} for Ag^+ and Hg^{2+} ions in **BHP**, respectively (ESI† Fig. S23). The fast response of the sensors to Ag^+ and Hg^{2+} ions makes them suitable for real-time detection in samples. The effect of reaction time on the sensor **MHC**/**BHP**-Ag^+/Hg^{2+} binding process was investigated, and it was found that the fluorescence intensity of the sensors reached equilibrium within 5 s (ESI† Fig. S24). Therefore, a reaction time of 5 s can be used for this sensing system, which implies that the sensor can be an excellent tool for the real-time detection of Ag^+ and Hg^{2+}.

2.6. Sensing mechanism

The **MHC** molecule exhibits ICT from the TSC unit to the phosphinine core, resulting in orange emission in fluorescence spectroscopy. Upon coordination with Ag^+/Hg^{2+} ions, the **MHC** molecule shows a blue shift and an enhanced emission due to the CHEF mechanism. The **BHP** molecule, which has a benzothiazole (BT) core instead of a TSC unit, displays a bright green fluorescence emission. However, when the **BHP** molecule binds to Ag^+/Hg^{2+} ions, it undergoes a red shift and reduced emission due to the CHEQ effects. The interaction mechanism between **MHC**/**BHP** and Ag^+/Hg^{2+} ions was investigated through a ^{1}H NMR titration experiment. Fig. 5a shows that the NH protons of **MHC** resonate at a downfield than expected from the deshielding effect of the adjacent electronegative atoms. This is because

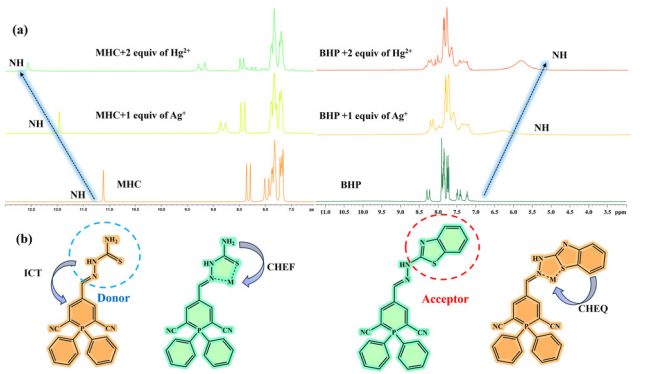

Fig. 5 ^{1}H NMR titration spectra of **MHC** and **BHP** after additions of Ag^+ and Hg^{2+} ions (0–2 equivalents) in DMSO-d_6. (b) Chemical structures of **MHC**, **BHP** and its complexes with Ag^+ and Hg^{2+} ions.

the nitrogen atom of the amine group participates in resonance with the TSC unit, acting as an electron-donating group by conjugation in **MHC**. When the nitrogen atom cannot participate in resonance forms, the nitrogen of the amine group acts as an electron-withdrawing atom by induction due to the higher electronegativity of nitrogen than that of carbon. Moreover, the magnetic field experienced by the nucleus depends on the electron density around the atom. Therefore, the lower the electron density around the TSC unit, the lower the field of the shift. When the electron density around the NH atom decreases, the magnetic field opposing it decreases, and then the nucleus feels more of an external magnetic field. Thus, the NH proton in **MHC** shows deshielding. In contrast, receptor **BHP** has a rotatable benzothiazole ring that may be stabilised by complexation with sulphur and a C═N group. After the complexation of **BHP** with Hg^{2+}/Ag^{+}, the NH peak shifts to a shielded field. This is because conjugation is still present and initiated by the BT unit. When the electron density of the **BHP** is high around the BT unit, the magnetic field opposing it is also high, which in turn causes shielding of the NH proton. To understand how the sensing process works, we need to know how the chemosensor and analyte react with each other in a stoichiometric ratio. We used Job's plot-based analysis to determine this ratio for the sensors **MHC** and **BHP** with Ag^{+}/Hg^{2+} ions. We kept the same quantity of the sensor **MHC** and **BHP** solution with Ag^{+}/Hg^{2+} ions in each experiment, which was 2×10^{-5} M. We observed that the highest change in fluorescence intensity occurred when the ratio of the sensor and the ion was 0.5, which means that they formed a 1 : 1 complex (ESI† Fig. S25). Similarly, we confirmed this result with HRMS spectral analysis. The result showed us the mass of the 1 : 1 complex between **MHC** and **BHP** with Ag^{+}/Hg^{2+} ions. The HR-MS spectra of **MHC** and **BHP** showed MS peaks at m/z = 402.0915 and m/z = 476.1098, corresponding to $[(\mathbf{MHC}) + H]^{+}$ and $[(\mathbf{BHP}) + H]^{+}$, respectively (ESI† Fig. S10 and S14). When 2 equivalents of Hg^{2+} were added to **MHC** and **BHP**, new peaks at m/z = 727.0403 and 801.0482 were observed for (**MHC** + Hg^{2+}) and (**BHP** + Hg^{2+}), respectively, indicating the formation of a 1 : 1 complex of **MHC** and **BHP** with Hg^{2+} (ESI† Fig. S26 and S27). Similarly, when 2 equivalents of Ag^{+} were added to **MHC** and **BHP**, the original peak at m/z = 402.0915 for **MHC** and m/z = 476.1098 for **BHP** disappeared, and a new peak at m/z = 570.9869 for $[(\mathbf{MHC} + Ag^{+}) + H]^{+}$ and m/z = 666.9846 for $[(\mathbf{BHP} + Ag^{+}) + Na]^{+}$ appeared, suggesting the formation of a 1 : 1 complex of **MHC** and **BHP** with Ag^{+} (ESI† Fig. S28 and S29). Furthermore, **MHC** and **BHP** were tested for their fluorescence quantum yield (Φ_{fl}) relative to quinine sulfate (Φ_{fl} = 0.54 in 0.5 M conc. H_2SO_4). The obtained quantum yields for **MHC** and **BHP** are 89% and 65%, respectively.

2.7. Computational analysis

In this study, we used the density functional theory (DFT) method to study the most likely three-dimensional (3D) structure of **MHC**, **BHP**, and their complexes with Ag^{+} and Hg^{2+} ions based on experimental data. For the DFT computations, the computer programme Gaussian 16 package was used, and the atoms of C, H, S, and N were represented using the B3LYP exchange–correlation functional and the basis sets 6-31G, while metal ions were represented using the LANL2DZ basis set. The aforementioned strategy was used to optimize the overall structure of sensors **MHC** and **BHP**, as well as to understand how they interact with Ag^{+} and Hg^{2+} ions. ESI† Fig. S30 displays the structure of the sensors. The most plausible transitions between **MHC** and **BHP** towards their complexes, together with their oscillator strengths and transition motion, are displayed in ESI† Table S3. According to ESI† Table S4 analyses, the energy gap (E) between the HOMO and LUMO of **MHC**/**BHP** and their complexes with Ag^{+}/Hg^{2+} was calculated. A detailed evaluation of the MO diagram in ESI† Fig. S31a and b indicates that the electron density is localised in **MHC** and **BHP** for the highest occupied molecular orbital (HOMO) on the TSC unit and BT core. The nitrile-linked phosphinine moiety is located at the position of the lowest unoccupied molecular orbital (LUMO). In **MHC** and **BHP**-Ag^{+}/Hg^{2+} complexes, HOMO is positioned above the phosphinine ring to TSC in **MHC** and BT in **BHP**, similar to Ag^{+} and Hg^{2+} complexes. LUMO is completely filled with **MHC** and **BHP**-Ag^{+}/Hg^{2+} complexes. Specifically, the LUMO electron cloud density surrounding the phosphinine unit and metal complexes is observed in **BHP**-Ag^{+}/Hg^{2+} complexes. This causes NH to move towards the shielding region because of the electron density that forms surrounding it. As observed in (ESI† Fig. S31a and b), the **MHC** and **BHP** sensors are superior at stabilising Hg^{2+} ions over Ag^{+} complexed ligands. This suggests that the HOMO–LUMO gap is greater for Hg^{2+} complexes than for Ag^{+} complexes. According to the results (ESI† Fig. S31a), the HOMO–LUMO gap is greater for **MHC** + Hg^{2+} (3.61 eV) than for **MHC** + Ag^{+} (3.24 eV). ESI† Fig. S31b illustrates the same thing for **BHP** + Hg^{2+} (3.42 eV) and **BHP** + Ag^{+} (3.33 eV). If different metal ions coordinate with the molecules, the HOMO–LUMO energy gap shifts accordingly.

3. Utilising real-world applications

3.1. Reversibility behaviour of MHC and BHP

One of the most important requirements for an optimal fluorescent chemo sensor is good reversibility. Using the different analytes, we examined the sensitivity and reversibility of our synthesised **MHC** and **BHP** towards Ag^{+} and Hg^{2+} ions. Remarkably, it has been discovered that the behaviour of metal sensing is completely reversible when EDTA is present (ESI† Fig. S32). Compared to the **MHC** and **BHP**-Ag^{+}/Hg^{2+} complexes, EDTA forms a more stable complex owing to its strong reactivity with Ag^{+} and Hg^{2+} metal ions. By first introducing Ag^{+}/Hg^{2+} and subsequently EDTA, the red and blue shifts in emission appeared throughout the four cycles (ESI† Fig. S33). During these four cycles, there was a noticeable reversal in the shift in fluorescence emission and colour change. Consequently, it

exhibited fluorescence switching behaviour in the presence of EDTA, blue and red shifts in the emission spectrum in **MHC** and **BHP**, and colour changes from yellowish orange to green in **MHC** and bright green to orange in **BHP**. These data demonstrate that **MHC** and **BHP** are reversible, recyclable Ag^{+}/Hg^{2+} sensors and that their Ag^{+}/Hg^{2+} complexes function as secondary EDTA sensors.

3.2. Paper strip application

To investigate the practical use of the chemo sensors **MHC** and **BHP** ACN : H_2O (8 : 2) solution system, test strip detection tests were conducted. Sensors **MHC** and **BHP** were coated with 4 × 1.5 cm Whatman filter paper and allowed to dry. The result was a yellowish orange colour strip for **MHC** and a bright green colour strip for **BHP**, as shown in Fig. 6a and c. The **MHC** and **BHP**-loaded strips did not display any noticeable colour changes from any of the other metal ions. After being immersed in Ag^{+} ions, the paper strip transformed from yellowish orange to greenish yellow in **MHC** and bright green to orange in **BHP**. Similarly, upon being submerged in Hg^{2+} ions, the receptor-coated strip became green in **MHC** and muddy orange in **BHP** (Fig. 6a and c). In the presence of Ag^{+}/Hg^{2+}, we found exactly similar responses from **MHC** and **BHP** in the solution medium (Fig. 6b and d). Hence, to ascertain the probe's probable real-world applications, its practical applicability was observed.

3.3. Examination of Ag^{+} and Hg^{2+} ions in raw water collections

The practical application of **MHC** and **BHP** to evaluate Ag^{+} and Hg^{2+} cations was verified by their applicability in real-time water sample identification. We added known amounts of Ag^{+} and Hg^{2+} ions to water samples taken from various sources. The metal content of the generated samples was evaluated by recording their fluorescence spectra. The quantitative measurement of the supplied sensor matched the known spiking amounts of Ag^{+} and Hg^{2+} ions, as shown in Table 1. With a reduced relative standard deviation (n = 3), the **MHC** sensor demonstrated an exceptional recovery rate for Ag^{+} and Hg^{2+} ions, ranging from 95% to 102.5%. These results support the idea that **MHC** and **BHP** sensors are highly useful for identifying Ag^{+} and Hg^{2+} ions in water samples.

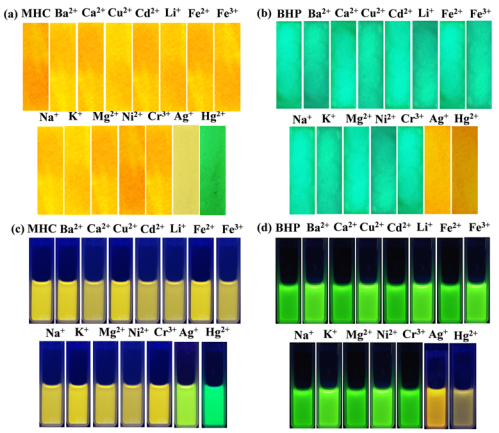

Fig. 6 Image demonstrating the (a) **MHC** and (b) **BHP** fluorescence colour changes that result from adding different metal ions to test paper strips at 365 nm. (b and d) Bottle images of **MHC** and **BHP** in the presence of the aforementioned metal ions.

3.4. Live cell visualization of MHC and BHP

In this study, we assessed the significance of utilizing the **MHC** and **BHP** fluorescent probes in a biological context. Specifically, these probes were employed for intracellular detection and monitoring of Ag^{+} and Hg^{2+} ions within HeLa cells, a cell line derived from Henrietta Lacks. To evaluate the cytotoxicity of these probes, we conducted an MTT assay shown ESI† Fig. S34a (**MHC**) and S34b (**BHP**). The results showed that when used at concentrations exceeding 10 μM, the cell viability remained high, with 95% for **MHC** and 94% for **BHP**. Following a 20-minute incubation of HeLa cells with 10 μM concentrations of **MHC** and **BHP**, we employed a confocal fluorescence microscope for cell imaging (Fig. 7b and h). The bio-imaging application involved the use of 10 μM concentrations of Ag^{+} and Hg^{2+}. Fig. 7d, f, j and i illustrate the *in vitro* fluorescence study of **MHC** and **BHP** with Ag^{+}/Hg^{2+} on HeLa cells. Notably, when HeLa cells were exposed to Ag^{+} ions in the presence of the **MHC** and **BHP** sensors, a noticeable shift in fluorescent colour was observed. **MHC** exhibited a transition from red to green fluorescence, while **BHP** shifted from bright green to red fluorescence. Similarly, the sole application of Hg^{2+} in the presence of **MHC** produced green fluorescence in HeLa cells, while **BHP** treated with Hg^{2+} ions resulted in intense red fluorescence. These findings correspond to the ratio metric fluorescence shift detected in solution-phase studies. It is important to note that the characteristic fluorescence emitted by the cells did not interfere with the analysis, as the probes exhibited their unique fluorescence behaviour.

Conclusion

We created, synthesised, and thoroughly examined two new phosphinine-based sensors, **MHC** and **BHP**, with quantum yields (Φ) of 89% and 65%, respectively, with AIE and ACQ activity and interestingly explored solvatochromism in photophysical phenomenon. Utilizing a synthesised sensor probe **MHC** and **BHP**, it was possible to detect Ag^{+} and Hg^{2+} ions more sensitively and selectively than other metal ions in a mixed aqueous solution ACN : H_2O (8 : 2) using both as fluorescence sensors. Remarkably, the fluorescence characteristics were changed by simply adding Ag^{+} and Hg^{2+} ions. Based on these ratiometric properties, a method was devised to selectively detect both ions with these sensor probes. Along with paper strip sensing, onsite detection of Ag^{+} and Hg^{2+} ions in actual samples was carried out owing to the paper strip sensor's selectivity and sensitivity of probe

Table 1 Detection of Ag^{+} and Hg^{2+} ions by employing **MHC** and **BHP** in various water samples

Sample	Sensor	Ion	Spiked (μM)	Found (μM)	Recovery[a] (%)	RSD (%, n = 3)
Tap water	**MHC**	Ag^{+}	0.2	0.192	96	0.2
			0.4	0.390	97.5	0.52
		Hg^{2+}	0.2	0.194	97	0.11
			0.4	0.392	98	0.40
	BHP	Ag^{+}	0.2	0.190	95	0.96
			0.4	0.391	97.75	0.97
		Hg^{2+}	0.2	0.193	96.5	0.49
			0.4	0.393	98.25	0.32
Lake water	**MHC**	Ag^{+}	0.2	0.196	98	0.44
			0.4	0.397	99.25	0.11
		Hg^{2+}	0.2	0.197	99	0.82
			0.4	0.398	99.5	0.53
	BHP	Ag^{+}	0.2	0.197	98.5	0.60
			0.4	0.395	98.75	0.57
		Hg^{2+}	0.2	0.196	98	0.63
			0.4	0.396	99	0.87
Industrial waste water	**MHC**	Ag^{+}	0.2	0.198	99	0.88
			0.4	0.410	102.5	0.68
		Hg^{2+}	0.2	0.198	99.1	0.46
			0.4	0.412	103	0.44
	BHP	Ag^{+}	0.2	0.199	99.5	0.20
			0.4	0.405	101.25	0.82
		Hg^{2+}	0.2	0.203	101.5	0.26
			0.4	0.410	102.5	0.50

[a] Mean ± SD of three replicate analysis.

MHC and **BHP** towards Ag^{+} and Hg^{2+} ions. Furthermore, a fluorescence bio-imaging experiment demonstrated that the sensors **MHC** and **BHP** could identify Ag^{+} and Hg^{2+} ions in living HeLa cells. This method can be applied to industrial processes to help keep the air and environment safe.

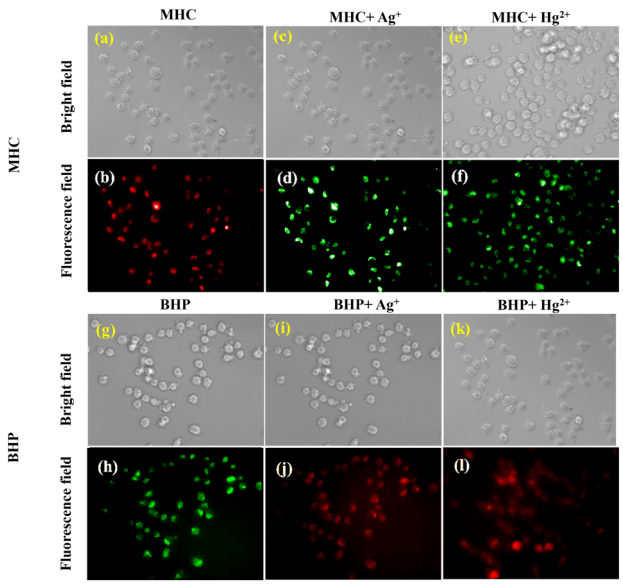

Fig. 7 Images of live HeLa cells subjected to **MHC** and **BHP** sensors in the presence of Ag^{+} and Hg^{2+} ions *via* fluorescence microscopy. The images (a, c and e) illustrate the bright-field microscopy of **MHC** and its complexes, while (b, d and f) highlight their fluorescent-field imaging. Similarly, (g, i and k) provide bright-field views of **BHP** and its complexes, complemented by the fluorescent-field perspectives in (h, j and l). The result were obtained using a 25 μm scale bar.

Data availability

The data supporting this article have been included as part of the ESI.†

Conflicts of interest

There are no conflicts to declare.

Acknowledgements

Saravanan Enbanathan is deeply grateful for the financial support he has received from VIT in the form of a Research Associateship. It is important to acknowledge the contribution of VIT-SIF to the characterization studies. For language polishing, the authors thank Dr. R. Srinivasan, VIT-SSL. The fluorescence bioimaging laboratory facility provided by Dr. R. Loganathan is gratefully acknowledged.

Notes and references

1 U. Balijapalli, S. Manickam, K. Thirumoorthy, K. Natesan Sundaramurthy and K. Iyer Sathiyanarayanan, *J. Org. Chem.*, 2019, **84**, 11513–11523.
2 S. K. Patra, S. K. Sheet, B. Sen, K. Aguan, D. R. Roy and S. Khatua, *J. Org. Chem.*, 2017, **82**, 10234–10246.
3 S. Enbanathan and S. K. Iyer, *Ecotoxicol. Environ. Saf.*, 2022, **247**, 114272.
4 P. Chinna Ayya Swamy, J. Shanmugapriya, S. Singaravadivel, G. Sivaraman and D. Chellappa, *ACS Omega*, 2018, **3**, 12341–12348.

5 S. Enbanathan, S. Munusamy, S. Ponnan, D. Jothi, S. Manoj Kumar and K. I. Sathiyanarayanan, *Talanta*, 2023, **264**, 124726.
6 A. Roy, M. Nandi and P. Roy, *TrAC, Trends Anal. Chem.*, 2021, **138**, 116204.
7 M. Dutta and D. Das, *TrAC, Trends Anal. Chem.*, 2012, **32**, 113–132.
8 J. Wang, J. Tong, Z. F. Wang, Q. Yuan, X. Y. Wang, S. Y. Yu and B. Z. Tang, *Anal. Chim. Acta*, 2022, **1208**, 339824.
9 M. Isaac, S. A. Denisov, N. D. McClenaghan and O. Sénèque, *Inorg. Chem.*, 2021, **60**, 10791–10798.
10 X. Wang, X. Gao, X. Lin, S. Zheng, Y. Yan, S. Wang and Y. Liu, *Spectrochim. Acta, Part A*, 2022, **268**, 120696.
11 Y. Min, X. Han, Y. Qi, L. Jiang, Y. Song, Y. Ma, J. Zhang and H. Li, *Color. Technol.*, 2023, **140**, 30–41.
12 K. Krishnaveni, M. Iniya, A. Siva, N. Vidhyalakshmi, S. Sasikumar, U. K. Pandian Ramesh and S. Murugesan, *J. Mol. Struct.*, 2020, **1217**, 128446.
13 S. Enbanathan, S. Manickam, M. Dhanthala Thiyagarajan, D. Jothi, S. Manojkumar, S. Munusamy, D. Murugan, L. Rangasamy, U. Balijapalli and S. Kulathu Iyer, *J. Photochem. Photobiol., A*, 2023, **437**, 114431.
14 Y. Han, C. Yang, K. Wu, Y. Chen, B. Zhou and M. Xia, *RSC Adv.*, 2015, **5**, 16723–16726.
15 S. Lei, X. Meng, L. Wang, J. Zhou, D. Qin and H. Duan, *ChemistryOpen*, 2021, **10**, 1116–1122.
16 Z. Wang, Y. Zhang, J. Yin, Y. Yang, H. Luo, J. Song, X. Xu and S. Wang, *ACS Sustainable Chem. Eng.*, 2020, **8**, 12348–12359.
17 T. H. Nguyen, T. Sun and K. T. V. Grattan, *Sensors*, 2019, **19**, 2142.
18 M. S. Hosseini and H. Hashemi-Moghaddam, *Talanta*, 2005, **67**, 555–559.
19 H. Li and H. Yan, *J. Phys. Chem. C*, 2009, **113**, 7526–7530.
20 R. Bhaskar and S. Sarveswari, *ChemistrySelect*, 2020, **5**, 4050–4057.
21 K. S. Jagadhane, S. R. Bhosale, D. B. Gunjal, O. S. Nille, G. B. Kolekar, S. S. Kolekar, T. D. Dongale and P. V. Anbhule, *ACS Omega*, 2022, **7**, 34888–34900.
22 P. Mohanty, P. P. Dash, S. Naik, R. Behura, M. Mishra, H. Sahoo, S. K. Sahoo, A. K. Barick and B. R. Jali, *J. Photochem. Photobiol., A*, 2023, **437**, 114491.
23 A. Panja and K. Ghosh, *New J. Chem.*, 2019, **43**, 5139–5149.
24 P. Thamaraiselvi, N. Duraipandy, M. Syamala Kiran and S. Easwaramoorthi, *ACS Sustainable Chem. Eng.*, 2019, **7**, 9865–9874.
25 U. Krishnan and S. K. Iyer, *Photochem. Photobiol.*, 2021, **98**, 843–855.
26 L. Huang, W. Sheng, L. Wang, X. Meng, H. Duan and L. Chi, *RSC Adv.*, 2021, **11**, 23597–23606.
27 D. Jothi and S. K. Iyer, *Inorg. Chem. Commun.*, 2022, **143**, 109735.
28 X. Tang, U. Balijapalli, D. Okada, B. S. B. Karunathilaka, C. A. M. Senevirathne, Y. Lee, Z. Feng, A. S. D. Sandanayaka, T. Matsushima and C. Adachi, *Adv. Funct. Mater.*, 2021, **31**, 2104529.
29 U. Balijapalli, X. Tang, D. Okada, Y. Lee, B. S. B. Karunathilaka, M. Auffray, G. Tumen-Ulzii, Y. Tsuchiya, A. S. D. Sandanayaka and T. Matsushima, *Adv. Opt. Mater.*, 2021, **9**, 2101122.
30 J. P. Nandre, S. R. Patil, S. K. Sahoo, C. P. Pradeep, A. Churakov, F. Yu, L. Chen, C. Redshaw, A. A. Patil and U. D. Patil, *Dalton Trans.*, 2017, **46**, 14201–14209.
31 S. Enbanathan, S. Munusamy, D. Jothi, S. Manoj Kumar, P. Seenu, M. Faizan Noor and S. Kulathu Iyer, *J. Mol. Liq.*, 2024, **404**, 124949.
32 S. M. Kumar, S. Munusamy, D. Jothi, S. Enbanathan and S. K. Iyer, *J. Mol. Liq.*, 2023, **373**, 121235.
33 S. M. Kumar, S. Munusamy, S. Manickam, D. Jothi, S. Enbanathan and S. K. Iyer, *J. Mol. Liq.*, 2023, **381**, 121828.
34 S. Enbanathan, S. Munusamy, D. Jothi, S. Manoj kumar, A. P. Gopal and S. KulathuIyer, *Dyes Pigm.*, 2022, **205**, 110514.